1994PASJ...46L.137M

PASJ: Publ. Astron. Soc. Japan **46**, L137–L140 (1994)

LETTER

Soft X-Ray Spectral Features in the Seyfert 1 Galaxy NGC4051

Tatehiro MIHARA,[1] Masaru MATSUOKA,[1] Richard F. MUSHOTZKY,[2]
Hideyo KUNIEDA,[3] Chiko OTANI,[4] Sigenori MIYAMOTO,[5] and Makoto YAMAUCHI[1]

[1] *The Institute of Physical and Chemical Research, 2-1 Hirosawa, Wako, Saitama 351-01*
E-mail(TM) mihara@cricket.riken.go.jp
[2] *Laboratory for High Energy Astrophysics, NASA/GSFC, Greenbelt, MD 20771, USA*
[3] *Department of Physics, Faculty of Science, Nagoya University, Chikusa-ku, Nagoya 464-01*
[4] *Institute of Space and Astronautical Science, 3-1 Yoshinodai, Sagamihara, Kanagawa 229*
[5] *Department of Earth and Space Science, Faculty of Science, Osaka University,*
1-1 Machikaneyama-cho, Toyonaka, Osaka 560

(Received 1994 January 31; accepted 1994 June 1)

Abstract

We report ASCA observations of NGC 4051 during the PV phase. The time averaged X-ray spectrum is not well fit by a simple power law with an iron K-emission line and shows significant absorption-edge features most probably due to O VII and O VIII and a strong soft excess. This is the first direct measurement of edges in the spectrum of this object and confirms that the X-ray spectrum of NGC 4051 is modified by a "warm" absorbing gas. The best fit underlying power law index in the 0.4–10 keV band is 1.88. A power law modified by a warm absorber model can partly explain the apparent soft excess and qualitatively fit the SIS spectrum. However, the addition of a black body of $kT \sim 0.1$ keV improves the fit considerably. The 90% upper limit on the width of the iron line is 460 eV FWHM. Applying the fluorescent iron line model from an accretion disk gives an upper limit of 20° for the inclination of the disk.

Key words: Galaxies: individual (NGC 4051) — Galaxies: Seyfert — Galaxies: X-rays

1. Introduction

One of the nearest Seyfert 1 galaxies, NGC 4051 ($z = 0.0023$), has been well studied in the X-ray band and shows intensity variability down to a time scale of several 100's sec (Marshall et al. 1983; Fiore et al. 1992; Kunieda et al. 1992; Matsuoka et al. 1990; Lawrence et al. 1985). At lower energies a soft excess above an extrapolation of the simple power law was indicated by the Einstein (Urry et al. 1989) and EXOSAT (Lawrence et al. 1985). While over a half of all hard X-ray selected Seyfert 1 galaxies show some soft excess below ~ 1 keV (Turner, Pounds 1989; Brinkmann et al. 1994), its origin is not well understood and there are many possible explanations of this phenomenon (Turner et al. 1991). ROSAT all sky survey also detected a soft X-ray excess in 90% of 58 Seyfert 1 galaxies (Walter, Fink 1994). A detailed analysis of the simultaneous Ginga and ROSAT observations (Pounds et al. 1994) has shown that the spectrum cannot be described by a two component model but requires, in the low spectral resolution ROSAT data, an absorption feature which can be modeled by a "warm absorber." However, the ROSAT data were not capable of distinguishing a number of possible models.

Seyfert galaxies generally show evidence of an iron K-line emission in the X-ray band (Nandra, Pounds 1994) and the iron K-line from NGC 4051 was detected by Ginga near 6.4 keV with $EW \sim 200$ eV (Fiore et al. 1992; Matsuoka et al. 1990; Nandra, Pounds 1994). The X-ray spectra of many Seyfert galaxies observed with Ginga require a spectral flattening or hard bump above ~ 10 keV (Matsuoka et al. 1990; Pounds et al. 1990). This feature is explained by Compton reflection with optically thick material or by a leaky absorber in the line of sight. The observed iron K-lines may well arise from fluorescence of the same material (Lightman, White 1988; George, Fabian 1991; Matt et al. 1991). However, this feature is weak in the spectrum of NGC 4051 (Pounds et al. 1994).

ASCA observations of the broad band (0.4–10 keV) X-ray spectrum with the unprecedented spectral resolution and sensitivity can provide further precise information concerning the spectral structure and variability of Seyfert galaxies. In this paper we will concentrate on the X-ray spectral structure of NGC 4051.

© Astronomical Society of Japan • Provided by the NASA Astrophysics Data System

1994PASJ...46L.137M

2. Observations

ASCA observed NGC 4051 from 1993 April 25 22:30 to April 26 21:30 with a net exposure time of 42 ks. The SIS (Solid-state Imaging Spectrometer) was operated in 4-CCD mode in the energy range of 0.4–10 keV with a time resolution of 16 s. The GIS (Gas Imaging Spectrometer) was operated in PH mode in the energy range of 0.7–10 keV with a time resolution of 100 ms. GIS was in a normal operation condition except that the spread discriminator was not optimized yet. More detail on ASCA and the detectors is presented elsewhere. Because of an error in satellite pointing, the image of the source fell into the dead region between two chips in SIS-1. Therefore, we used the data only from SIS 0 and GIS 2 and 3 for the present analysis.

3. Spectral Analysis

The data are selected above 5° from the earth horizon for both the SIS and GIS. The average Dark Frame Error (offset of zero point) of SIS was −2 ADU (A/D Unit) = −7 eV. More strict selections were carried out to check the effect of DFE, but the energy of iron K line in NGC 4051 did not change in bright or faint mode and in day or night time, which indicates that the change of DFE is negligible. We used the response matrices rsp1.1α for DFE = −2 ADU and jbldarf 0.5b. The data in both bright and faint modes were added together to get good statistics. The data are accumulated in a circle of 2′.5 radius. There were no contaminating sources stronger than 0.01 times the intensity of NGC 4051 within 20′. The background was taken at the off-source position in the same field of view. The intensity of the background was two orders of magnitude less than that of NGC 4051 at any energy concerned. The average source intensity was 5×10^{-11} erg s^{-1}cm^{-2} (0.4–10 keV), and 2×10^{-11} erg s^{-1}cm^{-2} (2–10 keV), which is roughly 1 mCrab and consistent with the range, (0.2–5) $\times 10^{-11}$ erg s^{-1}cm^{-2} (2–10 keV), seen by previous experiments.

3.1. *Iron K Line*

An iron K-line emission feature is seen in the raw spectra of both SIS and GIS. The energy (uncorrected redshift) and equivalent width of this line are $E = 6.45 \pm 0.04$ keV and $EW = 170 \pm 70$ eV (SIS) and $E = 6.32 \pm 0.14$ keV and $EW = 150 \pm 70$ eV (GIS). The errors shown in this paper are 90% confidence statistical errors without systematic effects. Since the energy scale of the spectra can still have an instrumental uncertainty as much as 1%, these results are consistent with a neutral iron line at the redshift of the galaxy. The observed equivalent width is consistent with previous results. The line width is 460 eV FWHM in the 90% confidence limit. Fitting an accretion disk iron line model (Fabian et al. 1989), gives an upper limit of 20° for the inclination of the disk, which represents an almost face-on configuration.

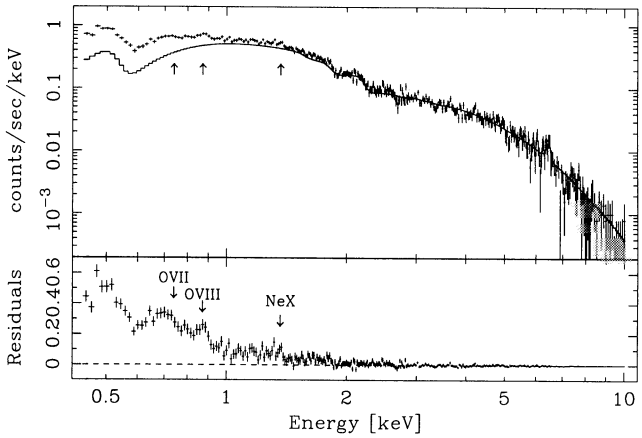

Fig. 1. X-ray spectrum observed with SIS 0. The curve is a single power law with galactic $N_{\rm H}$ of 1.3×10^{20} cm^{-2} and an iron line. Photon index is fixed to 1.88 which is the best-fit value in 2.5–6 keV band. Residuals from the model are shown in the lower panel. The arrows are at the expected edge energies.

3.2. *Photon Index of the Power Law*

We fit the observed spectrum to a single power law model with an iron K line over the energy range of 0.4–10 keV. The galactic $N_{\rm H}$ is fixed to 1.3×10^{20} cm^{-2} (Elvis et al. 1989) here and after. This model failed because of a large χ^2_ν (reduced χ^2 value) of 3.7 (dof=343), with the residuals showing an absorption-like or wavy structure around 1 keV. In order to obtain the photon index in the energy band similar to that of Ginga, we fitted the spectrum in the 2.5–6 keV range with a single power law. Since this energy band is above the Au M edges of the mirror, above Si K edge of the detector, and below the reflection component and an iron line, the response matrix is featureless and accurately known in this energy band. The photon index was 1.88 ± 0.10 (SIS) and 1.89 ± 0.08 (GIS). Ginga data showed an intensity dependence of the index (Matsuoka et al. 1990). According to the correlation, the intensity range observed with ASCA would correspond to a slope in the range 1.6–2.1 in the Ginga energy band, which is consistent with the ASCA result. Figure 1 shows SIS spectrum with the power law model with a fixed photon index of 1.88 and the residuals. The residuals suggest a waving structure around 1 keV and a clear soft excess below $\sim$ 1 keV.

© Astronomical Society of Japan • Provided by the NASA Astrophysics Data System

1994PASJ...46L.137M

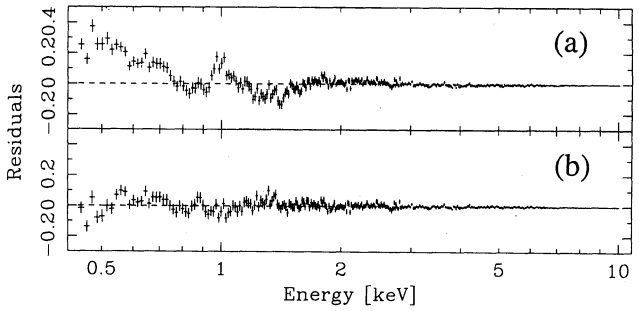

Fig. 2. (a) The residuals from a power law with a warm absorber, $\chi^2_\nu = 5.1$ (dof=343). The column density and ionization parameter of the warm absorber are log $N_{\rm H} = 23.2$ and $\log\xi = 2.7$. The photon index is fixed to 1.88, which is the best-fit value in 2.5–6 keV band. (b) The residuals from a power law with a warm absorber and a black body. A black body is added for the soft component. The best fit parameters are log $N_{\rm H} = 21.3 \pm 0.2$, $\log\xi = 1.7 \pm 0.2$, and $kT_{\rm bb} = 0.11 \pm 0.02$ keV giving $\chi^2_\nu = 1.30$ (dof=340). The best-fit model is shown in figure 3.

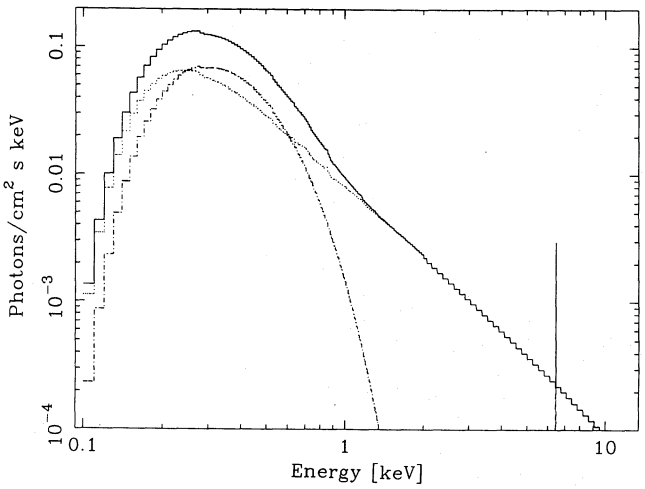

Fig. 3. The best-fit model for the SIS spectrum consisting of a single power law with a warm absorber, a black body for the soft component, an iron line, and a fixed galactic $N_{\rm H}$.

3.3. *Absorption Edge Feature*

Inspection of the residuals to the power law in figure 1 shows at least three edge-like structures at approximate energies of 0.74, 0.90, and 1.4 keV. Emission lines sometimes appear like edges, but there are no physically corresponding lines at the observed energies. In order to obtain their energies and optical depths, we fitted with a power law whose index was fixed to 1.88 and a black body (to account for the obvious soft excess) modified by three edges. The edge energies are 0.74 ± 0.02, 0.92 ± 0.02, and 1.4 keV (fixed) and optical depths 0.29 ± 0.08, 0.39 ± 0.11, and < 0.08, respectively. These edges probably correspond to K-edge absorptions by O VII (0.739 keV), O VIII (0.871 keV), and Ne X (1.362 keV) (Lotz 1968), which strongly suggests the existence of warm absorbing gas. This model leaves no significant features in the spectrum and the χ^2_ν was 1.32 (dof = 337) in the SIS fit.

The existence of these edges motivates the use of the "warm absorber" model. A model of the warm absorber was constructed using the "CLOUDY" photo-ionization code (Ferland 1991) and fitted to the SIS spectrum. The column density of the ionized absorber $N_{\rm H}$ [cm^{-2}] and ionization parameter $\xi = L/(nr^2)$ [erg s^{-1}cm] are set as free parameters, while the power law index is fixed to 1.88 and the redshift of the warm absorber is fixed to that of the galaxy. The χ^2_ν was 5.1 (dof=343) and the residuals are shown in figure 2a. The parameters are log$N_{\rm H}$ = 23.2, $\log\xi$ = 2.7. Some amount of the soft excess was explained by the warm absorber, but soft excess still remains as seen in the residuals.

3.4. *Soft Excess*

There are two ways to explain the remaining soft excess; to make the power law steeper or to add a soft component. If the power law index is varied, it converges to 2.28 ± 0.07 with the χ^2_ν of 1.53 (dof = 343). The best-fit parameters are log $N_{\rm H} = 22.2 \pm 0.2$, $\log\xi = 2.0 \pm 0.2$. The index does not overlap with 1.88 ± 0.10 in 2.3–6 keV, and it is steeper than the Ginga result (1.6–2.1).

Next, a black body radiation is added to the power law one with a fixed index 1.88. The χ^2_ν was 1.30 (dof = 340) and the residuals are shown in figure 2b. The best-fit model is shown in figure 3, whose parameters are log$N_{\rm H}$ = 21.3 ± 0.2, $\log\xi$ = 1.7 ± 0.2, and $kT_{\rm bb} = 0.11 \pm 0.02$ keV for the temperature of the black body. The best-fit flux of the warm-absorbed power law is 5.1×10^{-11} erg s^{-1}cm^{-2} (0.1–10 keV), and that of the black body is 1.6×10^{-11} erg s^{-1}cm^{-2} (0.1–2 keV). The black body component is not warm-absorbed in this model. But there would be no significant difference in the fitting if the black body component is warm-absorbed or not, because the flux of the black body is about 1/5 of the power law at warm edge energies. The model spectrum has corresponding edges to the data, but the depths of the edges do not always match. The residuals still show some structures below 2 keV. This could be understood considering that the present warm absorber model is a simple one, assuming uniform gas and temperature with solar abundances.

We successfully modeled this soft excess as either a black body of $kT_{\rm bb} = 0.11 \pm 0.02$ keV, a Raymond-Smith thermal spectrum with $kT_{\rm RS} = 0.17 \pm 0.02$ keV

© Astronomical Society of Japan • Provided by the NASA Astrophysics Data System

1994PASJ...46L.137M

and abundances $= 0.03 \pm 0.02$, a disk black body spectrum (Mitsuda et al. 1984) with $kT_{\rm in} = 0.14 \pm 0.03$ keV or a power law with index of 2.6 ± 0.5. All give similar χ^2_ν. The emission measure in the Raymond-Smith model is $n^2V \sim 3 \times 10^{64}$ cm^{-3} for an assumed disatance of 15 Mpc. This emission measure requires $r > 3 \times 10^{15}$ cm from the condition that $nr\sigma_{\rm T}$ is smaller than unity, where $\sigma_{\rm T}$ is the Thomson cross section. Though the total flux in the 0.2–2 keV band exhibits rapid time variability, there is no evidence of rapid variation of the soft component and thus thin thermal plasma models cannot be ruled out.

4. Discussion

The present results have revealed two significant absorption edges, probably due to O VII and O VIII, which is a direct evidence of a "warm absorber." Lower spectral resolution ROSAT observations have indicated a similar low energy spectral structure in some Seyfert galaxies and in a radio-loud quasar, 3C 351 (Fiore et al. 1993), which can be well modeled as an absorption edge at around 0.9 keV (Nandra, Pounds 1992; Nandra et al. 1993). Thus the presence of a "warm absorber" may be a common occurrence in the X-ray spectra of AGN. The smaller depth of the absorption in NGC 4051 in comparison to the case of MCG−6–30–15 (Fabian et al. 1994) shows that physical parameters exist in a wide range in these objects. The co-existence of O VII and O VIII edges suggests a non-uniform photo-ionization or a temperature structure. Some structure still remains in the spectrum below 2 keV. These unknown effects have to be investigated in detail with further observations of NGC 4051 and similar AGN's.

The apparent soft excess in NGC 4051 was partially explained by a warm absorber. An additional soft component improves the fitting. Simultaneous observations of NGC 4051 with Ginga and ROSAT (Pounds et al. 1994) showed that the dominant feature below 2 keV is well fitted by a warm absorber and a possible additional soft emission feature which can be modeled as a black body of $kT = 0.14$ keV. The ASCA results strongly supports the warm absorber and gives similar results for the soft component.

ASCA has detected a clear iron emission line at 6.45 ± 0.04 keV, which is consistent with the Ginga result. The upper limit of the width of 460 eV FWHM corresponds to the random velocity $< 10^9$ cm s^{-1}. The line centroid and relatively narrow width strongly constrain accretion disk models for the origin of the line (Matt et al. 1992). The upper limit on the line width indicates that most of the line flux comes from large radii ($R > 100R_{\rm s}$; $R_{\rm s}$: Schwarzschild radius) and that the system must close to face-on. This model predicts equivalent width < 100 eV, which is somewhat smaller than the ASCA values. The requirements that the iron line tracks the continuum on time scales of < 2000 s (Fiore et al. 1992) and $R > 100R_{\rm s}$ requires that the mass of the central object is less than $2 \times 10^6 M_\odot$.

References

Brinkmann W., Siebert J. 1994, A&A 285, 812

Elvis M., Lockman F.J., Wilkes B.J. 1989, AJ 97, 777

Fabian A.C., Kunieda H., Inoue S., Matsuoka M., Mihara T., Miyamoto S., Otani C., Ricker G. et al. 1994, PASJ 46, L59

Fabian A.C., Rees M.J., Stella L., White N.E. 1989, MNRAS 238, 729

Ferland G.J. 1991, Ohio State University, Astronomy Department Internal Report 91–01

Fiore F., Elvis M., Mathur S., Wilkes B.J., McDowell J.C. 1993, ApJ 415, 129

Fiore F., Perola G.C., Matsuoka M., Yamauchi M., Piro L. 1992, A&A 262, 453

George I.M., Fabian A.C. 1991, MNRAS 249, 352

Kunieda H., Hayakawa S., Tawara Y., Koyama K., Tsuruta S., Leighly K. 1992, ApJ 384, 482

Lawrence A., Watson M.G., Pounds K.A., Elvis M. 1985, MNRAS 217, 685

Lightman A.P., White T.R. 1988, ApJ 331, 57

Lotz W. 1968, J. Opt. Soc. America 58, 917

Marshall F.E., Holt S.S., Mushotzky R.F., Becker R.H. 1983, ApJL 269, L31

Matsuoka M., Piro L., Yamauchi M., Murakami T. 1990, ApJ 361, 440

Matt G., Perola G.C., Piro L. 1991, A&A 247, 25

Matt G., Perola G.C., Piro L., Stella L. 1992, A&A 257, 63

Mitsuda K., Inoue H., Koyama K., Makishima K., Matsuoka M., Ogawara Y., Shibazaki N., Suzuki K. et al. 1984, PASJ 36, 741

Nandra K., Fabian A.C., George I.M., Branduardi-Raymont G., Lawrence A., Mason K.O., M$^{\rm c}$Hardy I.M., Pounds K.A. et al. 1993, MNRAS 260, 504

Nandra K., Pounds K.A. 1992, Nature 359, 215

Nandra K., Pounds K.A. 1994, MNRAS 268, 405

Pounds K.A., Nandra K., Fink H.H., Makino F. 1994, MNRAS 267, 193

Pounds K.A., Nandra K., Stewart G.C., George I.M., Fabian A.C. 1990, Nature 344, 132

Turner T.J., Pounds K.A. 1989, MNRAS 240, 833

Turner T.J., Weaver K.A., Mushotzky R.F., Holt S.S., Madejski G.M. 1991, ApJ 381, 85

Urry C.M., Arnaud K., Edelson R.A., Kruper J.S., Mushotzky R.F. 1989, AGN and X-ray Background, Proc. 23rd ESLA Symposium, Vol.2 ed J. Hunt, B. Battrick, ESA, SP-296, p789

Walter R., Fink H. 1994, A&A 274, 105

© Astronomical Society of Japan • Provided by the NASA Astrophysics Data System